Fuzzy-based cooperative interaction between stand-alone microgrids interconnected through VSC-based multiterminal converter

Díaz, Nelson L.; Guinjoan, Francesc; Velasco-Quesada, Guillermo; Luna, Adriana C.; Guerrero, Josep M.

Published in:
International Journal of Electrical Power and Energy Systems

DOI (link to publication from Publisher):
10.1016/j.ijepes.2023.109226

Publication date:
2023

Document Version
Publisher's PDF, also known as Version of record

Electrical Power and Energy Systems 152 (2023) 109226

Contents lists available at ScienceDirect

International Journal of Electrical Power and Energy Systems

journal homepage: www.elsevier.com/locate/ijepes

Fuzzy-based cooperative interaction between stand-alone microgrids interconnected through VSC-based multiterminal converter☆

Nelson L. Díaz [a,*], Francesc Guinjoan [b], Guillermo Velasco-Quesada [c], Adriana C. Luna [d], Josep M. Guerrero [e]

[a] Universidad Distrital Francisco José de Caldas, Bogotá, 110231, Colombia
[b] Universitat Politécnica de Catalunya, Barcelona, 08034, Spain
[c] Universitat Politécnica de Catalunya, Barcelona, 08036, Spain
[d] Universidad de Puerto Rico, Recinto Mayaguez, Mayaguez, 00681, Puerto Rico
[e] Department of Energy Technology, Aalborg University, Aalborg, 9220, Denmark

ARTICLE INFO

Keywords:
VSC-based multiterminal
Microgrid energy exchange
Fuzzy inference systems
Stand-alone microgrids

ABSTRACT

This paper proposes a cooperative strategy for the flexible integration of stand-alone AC microgrids using an intermediate multiterminal DC link based on voltage source converters. The strategy manages cooperative power exchange between microgrids through a knowledge-based fuzzy inference system that relies on the current operating conditions of the microgrids. By determining the amount of power to be exchanged between microgrids to improve global reliability, the cooperative strategy achieves an overall reduction in load loss and an increase in the use of available renewable energy. Additionally, the multiterminal DC link provides complete isolation between microgrids, allowing for independent AC bus voltage regulation and management. The effectiveness and expandability of the proposed cooperative energy exchange strategy for enhancing the overall operation of multiple integrated microgrids have been fully verified by simulation and experimental validation.

1. Introduction

1.1. Motivation

Stand-Alone Microgrids based on renewable energy sources (RESs), such as photovoltaic (PV) generators or wind turbines (WT), in combination with energy storage systems (ESSs) have become a feasible solution for providing electricity to communities in remote areas [1,2]. Nevertheless, over time, the expected growth in energy demand may surpass the limit of energy availability in the remote microgrid [3]. This problem can be anticipated by oversizing the initial installation, which may result in an economically inefficient investment, or it could be compensated for by integrating more distributed generators [4]. This problem can be anticipated by oversizing the initial installation, which may result in an economically inefficient investment, or it could be compensated for by integrating more distributed generators [4]. As an alternative, several Stand-Alone microgrids can coexist, allowing for their electrical interconnection and energy exchange among them as part of a multi-microgrid cluster [5]. Even under grid-connected operation, geographically closer microgrids can cooperate in the event of an unexpected blackout in the main grid. Cooperative operation can enhance the global performance and reliability of individual microgrids, and reduce capacity requirements by taking advantage of different power balances between generation and consumption in the integrated power system [4]. In other words, a neighboring microgrid with a surplus of energy can provide energy support to another microgrid with an energy deficit [6].

The neighboring microgrids can be interconnected by means of a static switch or bidirectional interlinking converters based on multiple Voltage Source Converters (VSCs) linked by a DC bus, such as a back-to-back (BTB) converter [7–9]. While a static switch connection approach requires a dedicated communication system to ensure synchronization between microgrids, as well as a centralized supervisory unit responsible for managing power flow among microgrids, an interconnection through VSCs linked by a common DC link enables

☆ This work was partially supported by Minciencias with project Programa de Investigación en Tecnologías Emergentes para Microrredes Eléctricas Inteligentes con alta Penetración de Energías renovables, contract 80740-542-2020.

* Corresponding author.
E-mail addresses: nldiaza@udistrital.edu.co (N.L. Díaz), francesc.guinjoan@upc.edu (F. Guinjoan), guillermo.velasco@upc.edu (G. Velasco-Quesada), adriana.luna4@upr.edu (A.C. Luna), joz@et.aau.dk (J.M. Guerrero).

https://doi.org/10.1016/j.ijepes.2023.109226
Received 13 January 2023; Received in revised form 27 March 2023; Accepted 3 May 2023
Available online 15 May 2023

Nomenclature

(P^*)	Active Power Set Point
C_{BAT}	Battery Capacity
P_x	Active Power in Element x
V_{BAT}	Battery Voltage
V_{ED}	End of Discharge Voltage
V_r	Regulation Voltage
BTB	Back-To-Back
CoG	Center of Gravity
ESS	Energy Storage System
FCL	Fuzzy Logic Control
FIS	Fuzzy Inference System
H	High
$HVDC$	High Voltage Direct Current
L	Low
M	Medium
MFs	Membership Functions
$MGCC$	Microgrid Central Controller
MGs	Microgrids
N	Negative
NB	Negative Big
NM	Negative Medium
NS	Negative Small
P	Positive
PB	Positive Big
PM	Positive Medium
PS	Positive Small
PV	Photovoltaic
RES	Renewable Energy Source
SoC	State of Charge
VSC	Voltage Source Converters
WT	Wind Turbine
Z	Zero

asynchronous and independent operation of each AC power system [6,10–13]. In this way, each microgrid is able to continue operating as a self-controllable and autonomous entity, with its own management strategies, and keeping its autonomy to impose its own frequency and voltage regulation [14]. For instance, BTB converters are commonly used to interconnect AC microgrids with the utility grid, providing total frequency isolation, flexible power flow control, and a seamless transition between grid-connected and stand-alone operation [15–18]. Even if stand-alone microgrids are separated by long distances, interconnecting them with BTB-based HVDC systems can provide a more cost-effective and environmentally friendly solution [19].

1.2. Literature review

In light above, in [13] the authors present a review of multiple architectures and operation modes for interconnecting and managing clusters of microgrids. This work highlights the advantages of using power conversion units interconnected at a common dc bus, such as BTB, for the integration between multiple microgrids. In this sense, [6], and [20] explore the capability of BTB and multiterminal VSC-based converters for allowing energy exchange between stand-alone microgrids while providing frequency-dependent support from one grid to the other. Furthermore, in [9,11,21], and recently in [22] the authors present different versions of droop-based control schemes for BTB interlinks. The proposed droop schemes allow autonomous power flow through the BTB in order to balance the power in the linked stand-alone microgrids under changes in load or generation. Apart from that, recent research in this field has been focused on evaluating the stability of BTB for interlinking several ac and dc microgrids such as in [23], and also in exploring new and more efficient topologies for the BTB [24].

However, none of the previous contributions have addressed the challenge of managing the power exchange between multiple microgrids comprehensively. Those works have only considered for their studies Stand-Alone microgrids composed of generalized distributed generators with sufficient capacity and no limitations in order to test just the proper operation of the interlink converter. However, the main challenge arises when energy management has to deal with the highly intermittent and stochastic nature of renewable energy sources, as well as the limitations in storage units [25]. Few works have really approached this problem from this point of view, just in [26] the authors have considered the integration of two dc microgrids linked by an intermediate converter. Here, the power between the energy storage units in each microgrid is shared to enhance the performance and the overall storage capacity of the interlinked system. However, the group of interlinked microgrids is treated as a single power system where particular roles are assigned to each storage unit, which, in the end, makes difficult the expandability of the proposal, and the independent operation of each microgrid is completely lost. Also, in [27] a cooperative game approach has been proposed for achieving higher energy efficiency and operation economy for multiple grid-connected microgrids directly connected to the main grid. However, in the end, the multiple microgrid system is approached as a single aggregated system where the Stand-Alone microgrids lose their characteristic of being self-controllable and autonomous entities. Also, the cooperative integration of microgrid groups has been addressed from the point of view of the cybernetic layer by using multi-agent systems in which the convergence of the system is proven under a specific condition but intermittency a stochastic behavior of renewable generation has not been considered [28].

1.3. Contribution and paper organization

This paper aims to define a comprehensive cooperative energy exchange strategy between independent AC Stand-Alone microgrids with high penetration of renewable energy sources and limited energy storage capacity. The independent microgrids are integrated through a VSC-based multiterminal unit allowing for self and independent regulation and management of each microgrid while enabling the power exchange between microgrids. The proposed coordination strategy looks for enhancing global balance, reducing the loss of loads, and enhancing the use of renewable generation in the integrated microgrids.

The amount and direction of power exchanged between microgrids through the interlink VSC-based stage are defined by a knowledge-based Fuzzy Inference System (FIS). The FIS performs a real-time rule-based dispatch solely relying on current information about the available energy generation, consumption, and storage capacity of each microgrid, without requiring any prediction or optimized scheduling. In this way, it is possible to respond properly to operational uncertainties in RES generation. Fuzzy logic controllers have been widely used for the control and management of microgrids due to their ease of definition, relying on the user's experience rather than employing complex mathematical models of the system [29–31].

The proposed strategy proved to be expandable, allowing interconnection of more than two microgrids through the multiterminal converter. An advantage of the proposed coordination strategy is that it relies only on information with slow dynamic behavior, enabling the use of low-bandwidth communications between the microgrids and the management stage of the VSC-based multiterminal unit.

In this paper, Section 2 describes a general rule base management for the operation of each stand-alone microgrid and the operation of the VSC-based multiterminal unit. Section 3 presents the energy exchange strategy based on knowledge-based fuzzy inference systems used for

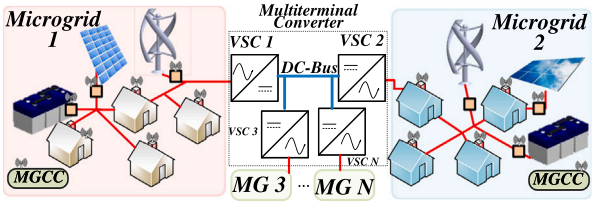

Fig. 1. Scheme of stand-alone microgrids linked by the VSC-based multiterminal stage.

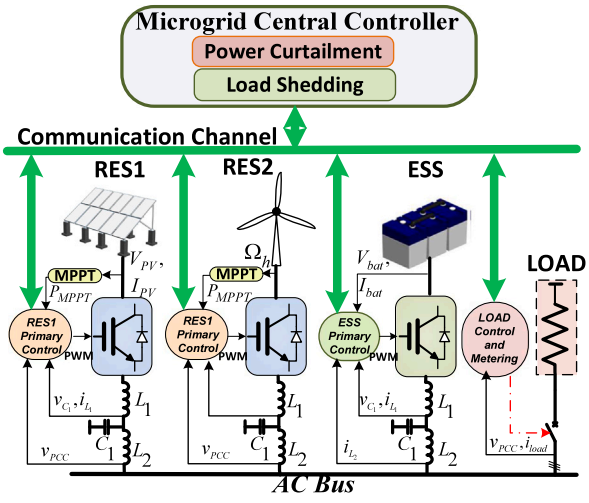

Fig. 2. Scheme of each individual stand-alone microgrid.

cooperative operation between interconnected microgrids. Initially, a complex rule-based strategy was defined that considered many different operating conditions for the generators, loads, and storage. This strategy was defined solely by relying on qualitative knowledge, resulting in strong subjectivity. However, specific and correlated parameters were identified, enabling the definition of a simplified and more effective rule-based strategy. In Section 3 the operation and expandability of the proposed coordination strategy are validated by simulation. Section 4 shows the experimental validation for two integrated microgrids. Finally, Section 5 presents the conclusions of this work.

2. Structure and operation of the integrated power system

Fig. 1 shows a scheme of an integrated power system that is composed of several (N) Stand-Alone AC microgrids (MGs) linked by a VSC-based multiterminal unit with a unique DC-bus.

For each microgrid a standard configuration has been selected, as shown in Fig. 2, which is based on hybrid PV-WT generation units, a battery-based ESS, and an aggregated load representing the total consumption. All the microgrids are connected to a common dc bus. To ensure reliable operation of its microgrids, each microgrid has its own independent microgrid central controller (MGCC). The MGCC is responsible for managing the operation of distributed resources and ensuring power balance in stand-alone power systems. Initially, for the purpose of facilitating analysis, two linked microgrids will be considered for explanation.

Fig. 3 represents the hierarchical control structure of a system composed of two microgrids linked by a Multiterminal converter. The primary level defines the control mode of each power converter in the system, which can be either voltage source or power source. In each microgrid (AC-Side), the ESS is responsible for regulating the common bus voltage and is thus controlled in voltage control mode. Meanwhile, RESs are expected to operate as power sources at their point of maximum power [32]. As a result, they are controlled in

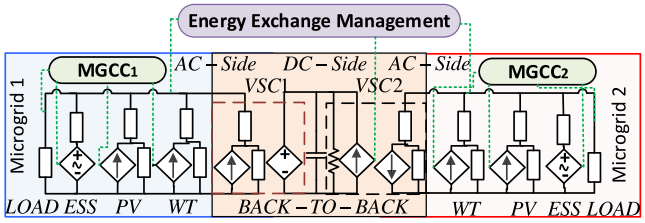

Fig. 3. Hierarchical control structure for two linked microgrids.

current control mode [33,34]. It is important to mention that, from the point of view of each AC microgrid, the corresponding VSC is seen as a power source or load. However, on the DC-side, the operation of the VSC is different. At least one of the VSCs should be operated in voltage control mode to ensure regulation of the DC bus, while the others can be controlled in current control mode to enable power flow. The voltage regulation task on the DC-side could be shared between two or more converters through the use of DC droop control loops [35]. At the next control level, the MGCCs work as supervisory stages in each microgrid with two main tasks. The first task is to limit the generation from RESs to prevent battery overcharge, and the second task is to disconnect the load whenever necessary to avoid battery over-discharge. Finally, the upper control level (Energy Exchange Management) manages the multiterminal in order to enable energy exchange between the two microgrids allowing their integrated and cooperative operation.

2.1. Operation of the MGCC in each stand-alone microgrid

A simple and centralized rule-based energy management strategy, previously presented in [36] and [37], was implemented in the MGCCs [38] for testing independent operation of the microgrids. This strategy is based on the limitations of battery-based ESS, as lead–acid and Li-ion batteries are the most commonly used for integrating RES [39]. The maximum and minimum charge limits for the ESSs are defined by voltage levels [40]. Specifically, the regulation voltage (V_r), which corresponds to approximately 90% of the battery State of Charge (SoC), and the end-of-discharge voltage (V_{ED}), which corresponds to approximately 20% of the battery SoC [39,41]. These values are generally provided by the manufacturers [42]. The MGCC coordinates two main actions:

1. **Power curtailment:** If the generation from RESs ($P_{RES} = P_{PV} + P_{WT}$) is higher than the consumption and the battery has reached its maximum charge limit (i.e., $V_{BAT} \geq V_r$), the generation from RESs is curtailed to prevent battery overcharging.
2. **Load Shedding:** When the generation RESs is lower than consumption and the battery has reached its minimum limit of charge (i.e. $V_{BAT} \leq V_{ED}$), the load should be disconnected for avoiding batteries deeper discharge.

The operation of the Stand-Alone microgrid depends on the information received from the distributed resources and the limits of charge of the battery-based ESS. Based on this, the microgrid can operate in three modes.

1. **Mode I:** The ESSs maintain the power balance in the system by charging or discharging based on the difference between generation and consumption ($P_{ESS} = P_{RES} - P_{LOAD}$). If the battery reaches its maximum or minimum charge state, the microgrid's operation changes to Mode II or Mode III, respectively.
2. **Mode II:** When the ESS reaches its maximum level of charge, power generation from each RES is curtailed proportionally to their maximum available power (P_{MP}) in order to achieve power balance ($P_{RES} = P_{LOAD}$) [36]. Once generation (P_{RES}) becomes smaller than consumption (P_{LOAD}), the microgrid operation returns to Mode I.

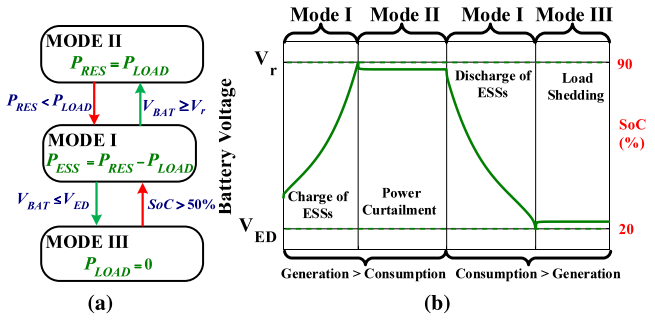

Fig. 4. Operation modes of a microgrid: (a) State diagram, (b) Battery voltage profile.

Table 1
Parameters of the stand-alone microgrid.

Parameter	Symbol	Value
Power System Stage		
Nominal Load	$P_{LOAD_{MAX}}$	2 kW
Maximum Power from RES	$P_{RES_{MAX}}$	2 kW
Nominal Bus Voltage	E^*	$230 * \sqrt{2}$ V
Nominal Bus Frequency	f^*	50 Hz
Inverter inductors	$L1, L2$	1.8 mH
Filter Capacitors	C	27 μF
ESSs Parameters		
Nominal Voltage	$V\,Bat$	720 V
Regulation Voltage	Vr	747 V
End-of-discharge voltage	V_{ED}	685 V
Maximum SoC	SoC_{MAX}	90%
Minimum SoC	SoC_{MIN}	20%
Battery Capacity	C_{BAT}	15 Ah
charging/discharging efficiency	η_{bat}	0.9
Maximum power for ESSs	$P_{ESS_{MAX}}$	± 2 kW

3. **Mode III:** The ESS has reached its minimum critical level of discharge and the load is disconnected to avoid deeper discharge. The load will be reconnected, and the microgrid will return to Mode I when the SoC of the battery exceeds a threshold value. In this case, a threshold value of 50% has been selected for the load reconnection since it is an intermediate value between the maximum and minimum levels.

Fig. 4(a) shows the scheme of the rule-based management that is deployed in the MGCCs, while Fig. 4(b) illustrates the charging profile used for a Li-ion battery in relation to the operation modes. In this case, to avoid overcharging, it is preferred to completely cut off the current charging the battery once the maximum voltage limit has been reached. This charging profile is preferred for Li-ion batteries to keep the battery voltage below its maximum limit [40].

In order to test the operation of the rule-based energy management on the MGCCs, two microgrids with two different generation and load profiles have been simulated as shown in Fig. 5 for a time-span of 24 h. The main parameters of the microgrids, which are the same for all the microgrids considered in this study, are summarized in Table 1 for the sake of simplicity.

Fig. 5(a) shows the response of Microgrid 1 (MG1), and it can be seen that the battery-based ESS sweeps all its operating range. Consequently, the microgrid operates under the three operation modes defined before. In MG1, the load is disconnected when the ESS reaches its minimum voltage level, and the power from RESs is curtailed when the ESS reaches its maximum limit of operation. In contrast, Microgrid 2 (MG2) always operates in Mode I, and the ESS uses less than half of its capacity (Fig. 4(b)). Under this scenario, MG2 could potentially provide

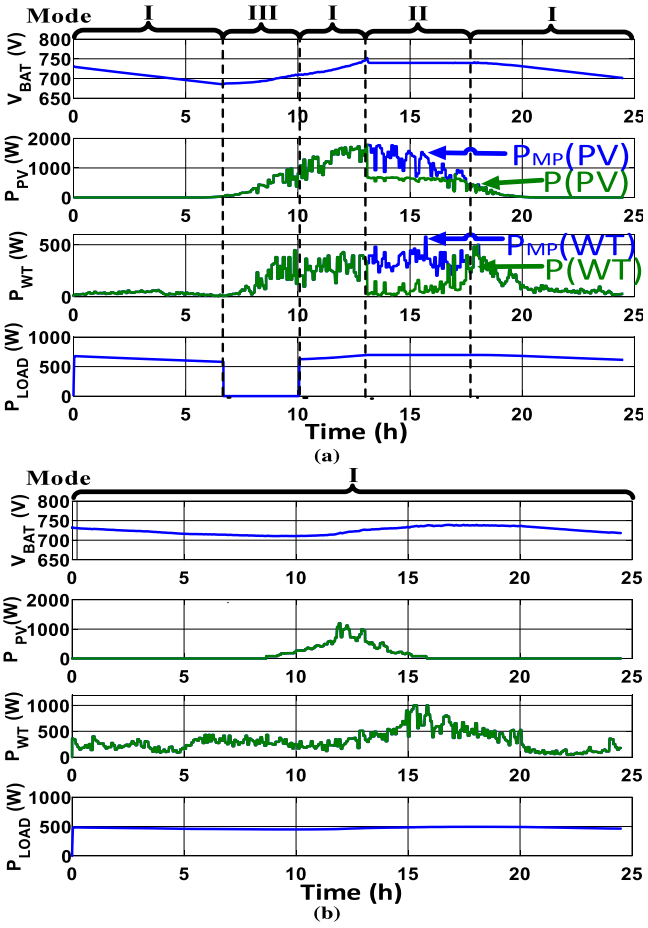

Fig. 5. Operation profile of each stand-alone microgrid with only local management: (a) Microgrid 1 (MG1), (b) Microgrid (MG2).

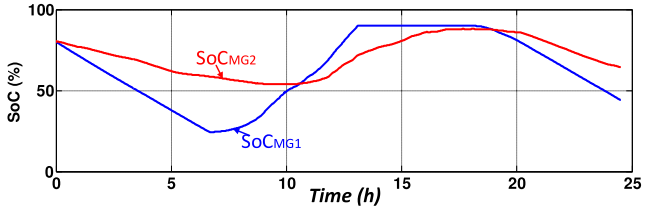

Fig. 6. Comparison between SoC in both microgrids.

energy to MG2 in order to prevent load loss between hours 5 and 10, and it could also store more energy between hours 12 and 17 for more efficient use of available resources. Fig. 6 shows a comparison between the behavior of the SoCs in MG1 (SoC_{MG1}) and MG2 (SoC_{MG2}). It can be noticed how the cycle depth of the ESS of MG1 is larger than the cycle depth of the ESS of MG2 since MG1 operates under extreme operation conditions while MG2 operates under a partial SoC.

2.2. VSC-based multiterminal, control and operation approach

Fig. 7 shows the suggested control block-diagram of the VSC-based multiterminal stage for two microgrids. This configuration can be expanded to include more microgrids. As mentioned before, at least one of the VSCs is responsible for regulating the intermediate DC-bus, while the others regulate the power flow between microgrids in accordance with the active power setpoints (P^*) defined by the Energy Exchange Management stage [20,43]. In Fig. 7, the exchange switch represents

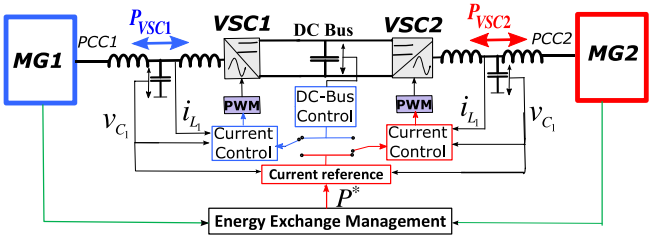

Fig. 7. Configuration of a two-terminal VSC-based unit.

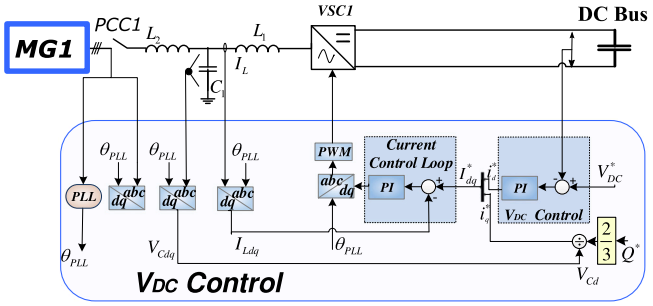

Fig. 8. Control scheme for the VSC1 (DC bus regulation).

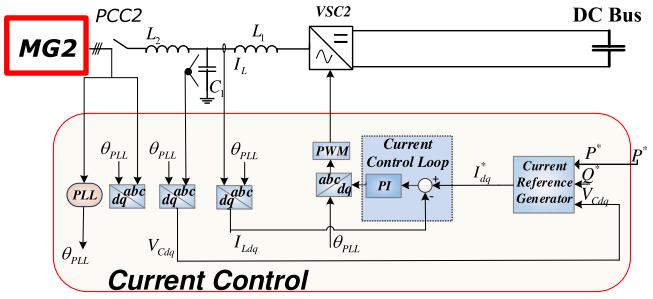

Fig. 9. Control scheme for the VSC2 (power flow control).

that the DC-bus control or power flow control can be assumed by any of the VSCs in the multiterminal converter. It is important to define which microgrid will assume these roles before beginning power exchange, and ideally, the microgrid with more storage capacity should be responsible for DC-bus regulation. For this study, the VSC connected to MG1 is responsible for regulating the DC Bus, while the VSC connected to MG2 controls the power flow. However, these control task assignments can be exchanged between the two VSCs. Figs. 8 and 9 illustrate the control-loop schemes for each VSC. As shown in Fig. 3, from the perspective of each microgrid's AC side, the VSC is controlled as a current source that is fully synchronized with the corresponding AC grid.

3. Energy exchange strategy

Figs. 5(a) and 5(b) demonstrate that, during a load disconnection in MG1, MG2 has sufficient energy to supply the load if both microgrids cooperate in sharing their energy resources. In this regard, the next section presents a comprehensive cooperative approach aimed at improving the global performance of the integrated group of microgrids.

3.1. Energy exchange based on a qualitative knowledge base

A basic cooperative strategy mainly requires the simultaneous knowledge of the following issues:

1. If any, which microgrid requires or can provide energy support.
2. What amount of support can be provided without violating the operation limits of the supporting microgrid (i.e. battery SoC upper and lower limits).

As a matter of fact, all this information can be obtained from the batteries. Indeed, the battery regulates the power balance, $P_{ESS_{MGi}}$ in each microgrid, defined as:

$$P_{ESS_{MGi}} = P_{CONS_{MGi}} - P_{GEN_{MGi}} \, for \; i = 1, 2, \ldots \tag{1}$$

Here, $P_{CONS_{MGi}}$ and $P_{GEN_{MGi}}$ refer to the power consumption and generation, respectively, of the ith microgrid. Therefore, the instantaneous power of the battery provides information about:

(a) If the microgrid generation is higher than the consumption (i.e., the battery is being charged with negative battery power) or lower than the consumption (i.e., the battery is being discharged with positive battery power), the microgrid can either deliver energy or require energy support.

(b) The amount of the battery power gives us information about the immediate future trend of the microgrid energy balance (production or consumption trends).

In addition, the battery SoC gives the information of its autonomy level, i.e. the amount of energy it can receive/deliver without violating its operating limits. Formally, this strategy requires just 4 inputs namely the instantaneous values of both the power and the SoC of the batteries of each microgrid. These inputs are respectively noted as $P_{ESS_{MG1}}$, $P_{ESS_{MG2}}$, SoC_{MG1}, and SoC_{MG2}. Therefore, each microgrid should only communicate two values to the energy exchanger unit.

The output of the strategy is the amount of incremental power, noted as ΔP^* to be transferred from the supporting microgrid to that requiring the support. By convention, this work considers that a positive value of ΔP^* means that energy is transferred from MG1 to MG2 and vice versa for a negative one.

A priori, it seems difficult or arbitrary to establish an analytical relationship between input and output variables that define the strategy for computing this amount under different operating conditions. However, it is easier to qualitatively define the energy exchange strategy by means of IF-THEN rules, as follows:

- If SoC_{MG1} is *High* and SoC_{MG2} is *High* and $P_{ESS_{MG1}}$ is *Positive Big* and $P_{ESS_{MG2}}$ is *Positive Big* then ΔP^* is *Zero*.
  This rule applies to an operating condition where the consumption in both microgrids is much greater than the generation ($P_{ESS_{MG1}}$ and $P_{ESS_{MG2}}$ are both significantly positive) and both ESSs have sufficient stored energy (SoC_{MG1} and SoC_{MG2} are both high). The strategy assumes that each ESS can maintain power balance within its respective microgrid, and there is no need for power transfer between the microgrids. Therefore, ΔP^* is zero.
- If SoC_{MG1} is *High* and SoC_{MG2} is *High* and $P_{ESS_{MG1}}$ is *Negative Big* and $P_{ESS_{MG2}}$ is *Positive Big* then ΔP^* is *Positive Big*.
  This operating condition arises when there is an imbalance between the microgrids, and both ESSs have sufficient stored energy (SoC_{MG1} and SoC_{MG2} are both high). In this case, MG1 generates much more power than it consumes ($P_{ESS_{MG1}}$ is significantly negative), while the opposite occurs in MG2 ($P_{ESS_{MG2}}$ is significantly positive). The strategy assumes that MG1 can transfer a large amount of power to MG2 (ΔP^* is significantly positive). It is worth noting that this rule is implicitly oriented towards preserving the SoC of the ESS in MG2, which would be used to ensure the individual power balance of MG2 in the absence of cooperation. Consequently, the cycling of the batteries is reduced, and their lifetime is preserved.

- If SoC_{MG1} is *Low* and SoC_{MG2} is *High* and $P_{ESS_{MG1}}$ is *Negative Medium* and $P_{ESS_{MG2}}$ is *Positive Big* then ΔP^* is *Negative Big*.
  Another operating condition where the cooperation strategy can be useful is when MG1 generates a slightly higher amount of energy than it consumes ($P_{ESS_{MG1}}$ is moderately negative), and its ESS is close to its lower limit (SoC_{MG1} is low), as this rule states. The strategy assumes that if the ESS in MG2 has sufficient energy (SoC_{MG2} is high), a large amount of power is transferred from MG2 to MG1 (ΔP^* is significantly negative), even if the consumption is much greater than the generation ($P_{ESS_{MG2}}$ is significantly positive). Note that the strategy in this case helps charge the ESS in MG2 to prevent its SoC from reaching its lower limit.
  Similarly to the previous rules, many others can be defined for different operating conditions.

The qualitative description can be transformed into a computational algorithm using the principles of Fuzzy-Based-Inference Systems (FIS) [44], also referred to as Fuzzy Logic Control (FLC). In essence, the design of such a system mainly addresses the following parameters:

(a) The membership functions (MF) of input and output variables play a crucial role in FIS design. These MFs are identified with linguistic labels, such as Negative Big (NB), and are responsible for quantifying, between 0 and 1, how true a physical value of an input variable can be considered as "Positive Big". The parameters of these MFs include the type, which is typically piece-wise linear, the number of inputs, and their mapping in a normalized range of the physical input values. It is noteworthy that the assignment of membership functions constitutes a mapping of the input design space, and subsequently, a corresponding assignment of control actions.

(b) The IF-THEN rule-base is a key component in defining the energy exchange strategy for the microgrids. This rule-base consists of a set of IF-THEN statements that map input variables to output variables, determining the appropriate control actions to be taken based on the current operating conditions.

(c) The choice of inference and defuzzification operators is critical for determining the output value based on the input variables according to the set of rules that define the strategy. In this work, we use the classical operators in FIS, which correspond to the Madmani inference method and the center of gravity (CoG) defuzzification method [45].

The FIS design process primarily focuses on points (a) and (b) and typically involves a simulation-based trial and error procedure for adjusting the strategy parameters using CAD tools such as the Fuzzy Toolbox of MATLAB. In the case under study, this process resulted in the following final design:

1. The same 5 MFs are used for the inputs $P_{ESS_{MG1}}$ and $P_{ESS_{MG3}}$, labeled as NB, NM, Z, PM, PB, where "N" stands for Negative, "P" for Positive, "Z" for Zero, "M" for Medium, and "B" for Big. The type and mapping of these MFs in a normalized domain are shown in Fig. 10(a). The same 3 MFs are used for the inputs SoC_{MG1} and SoC_{MG2}, labeled as L, M, and H, standing for Low, Medium, and High, respectively. The type and mapping of these MFs in a normalized domain are shown in Fig. 10(b).
2. Seven MFs were used for the output ΔP^*, labeled as NB, NM, NS, Z, PS, PM and PB, where S stands for "Small". The type and mapping of these MFs in a normalized domain are shown in Fig. 10(c). It can be noted in this case that these MFs are represented as singletons to simplify the computational complexity of the CoG defuzzification method [45].

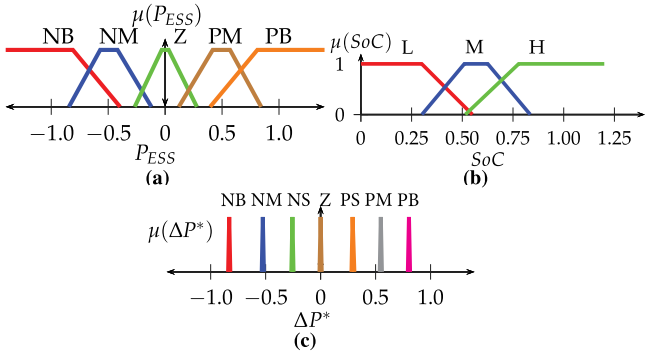

Fig. 10. Fuzzy sets for Inputs and outputs of the FIS.

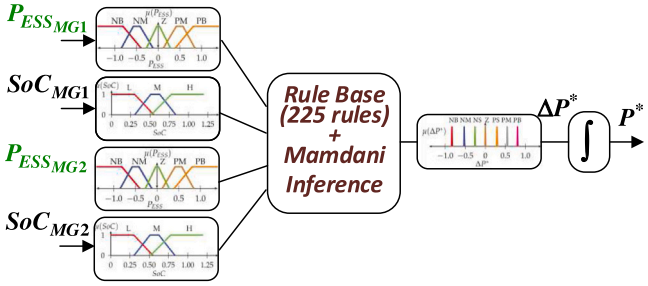

Fig. 11. Scheme of the fuzzy controller.

Fig. 11 shows the block diagram of the fuzzy controller in the Energy Exchange Management Unit, including the 225 rules resulting from all the possible combinations of the input MF ((3 for SoC_{MG1}) X (5 for $P_{ESS_{MG1}}$) X (3 for SoC_{MG2}) X (5 for $P_{ESS_{MG2}}$) = 225 *If-Then* rules). Table 2 maps the 225 combinations derived into the fuzzy rules.

Fig. 12 shows the response of MG1 and MG2, for a time-span of 24 h, interconnected through the multiterminal converter, and controlled by the defined FIS in the energy exchange management unit. In contrast with the behavior under independent operation shown in Fig. 5, it can be seen that:

(a) Both loads are supplied during the entire operation, therefore the overall system reliability is improved (no load disconnection in MG1).

(b) The RES generation is better exploited since **the curtailed RES energy is 42% less** than in the case of microgrids independent operation.

Fig. 13 also presents the evolution of the SoC profiles and the power exchanged between the two microgrids through the conversion stage (P_{VSCi}). Positive values of P_{VSCi} indicate that the ith microgrid is receiving energy, while negative values indicate that it is delivering energy. As expected, $P_{VSC1} \approx -P_{VSC2}$.

Comparing the SoC responses of Figs. 13 and 6, it is evident that under the cooperative strategy, the operation of both batteries remains within safe limits. Additionally, the depth of discharge for the ESS in MG1 is reduced compared to independent operation. Fig. 13 also shows that at the start of the day, MG2 supplies energy to MG1 to support its load and reduce the discharge of its battery. From Fig. 13, it can be observed that in addition to providing energy support to supply the loads, the energy exchange strategy aims to equalize the SoCs of both microgrids.

Table 2
Rule base of the FIS.

$P_{ESS_{MG1}}$	SoC_{MG1}									$P_{ESS_{MG2}}$
	H			M			L			
	Z	PS	PM	Z	Z	PS	NM	Z	Z	PB
PB	Z	PM	PM	NS	Z	Z	NM	NS	Z	PM
PB	NM	NS	Z	NM	NS	Z	NB	NS	Z	Z
PB	NM	NM	Z	NB	NB	Z	NB	NM	NS	NM
PB	NB	NM	NS	NB	NM	NS	NB	NM	NS	NB
PM	Z	PS	PS	NS	Z	PS	NM	NS	Z	PM
PM	Z	PS	Z	NM	NS	Z	NB	NS	Z	Z
PM	NS	Z	Z	NB	NS	Z	NB	NM	NS	NM
PM	NS	Z	Z	NB	NM	Z	NB	NM	NS	NB
Z	PM	PS	PB	Z	PS	PM	Z	Z	Z	PB
Z	PS	PS	PM	Z	PS	PS	NS	Z	Z	PM
Z	Z	Z	PM	NS	Z	PS	NM	NS	Z	Z
Z	Z	Z	PM	NM	Z	PS	NM	NS	Z	NM
Z	NS	Z	PS	NM	Z	Z	NM	NM	NS	NB
NM	PS	PM	PM	PS	PS	PB	Z	Z	PS	PB
NM	PS	PS	PS	Z	PS	PM	NS	Z	PS	PM
NM	PS	PS	PS	Z	Z	PS	NM	Z	Z	Z
NM	Z	Z	PS	Z	Z	Z	NB	NS	Z	NM
NM	Z	Z	PS	NS	Z	Z	NB	NS	Z	NB
NB	PB	PB	PB	PM	PM	PB	Z	Z	PM	PB
NB	PM	PM	PB	PS	PS	PM	Z	Z	PS	PM
NB	PM	PS	PB	Z	PS	PM	NS	Z	PS	Z
NB	PS	Z	PM	NS	Z	PS	NM	NS	Z	NM
NB	Z	Z	PS	NM	Z	PS	NM	NM	Z	NB
	H	M	L	H	M	L	H	M	L	
	SoC_{MG2}									

3.2. Simplified fuzzy inference system

The fact that SoC equalization is performed despite the differences in generation and consumption profiles suggests that the FIS can be simplified if the strategy directly aims for this equalization. In this case, considering only the difference between the SoCs of the batteries ($\Delta SoC = SoC_{MG1} - SoC_{MG2}$) as an input for the strategy rules would be sufficient, instead of using the two values of the SoCs. This approach would reduce the number of inputs and consequently, the number of rules, resulting in a lower computational complexity for the FIS. Moreover, as pointed out in Section 3.1, the sign of the power balanced by the ESS in each microgrid, noted as $Sign(P_{ESS_{MG1}})$ and $Sign(P_{ESS_{MG2}})$ gives information as to which microgrid is able to support the other one. Taking into account these previous considerations, a simplified FIS has been designed to implement an energy exchange strategy, which directly looks for the SoC equalization of both ESS, namely:

$$\Delta SoC = SoC_{MG1} - SoC_{MG2} = 0 \tag{2}$$

Following the same design steps as in Section 3.1, the resulting simplified FIS includes three inputs: (ΔSoC), ($Sign(P_{ESS_{MG1}})$, and

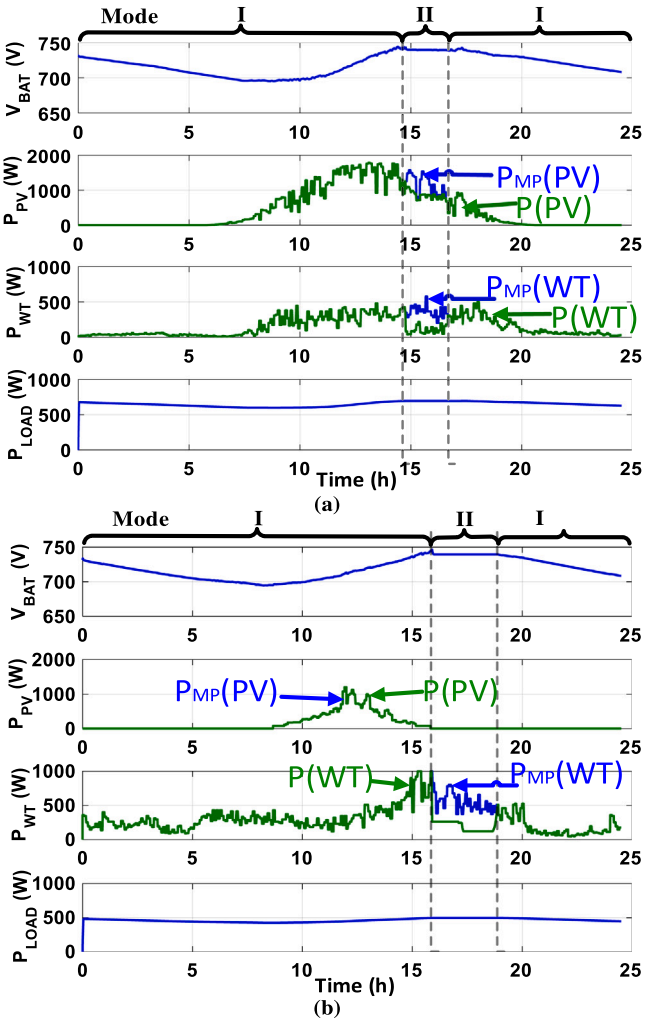

Fig. 12. Figures (a) and (b) show the operation of MG1 and MG2, respectively, using the fuzzy energy exchange strategy.

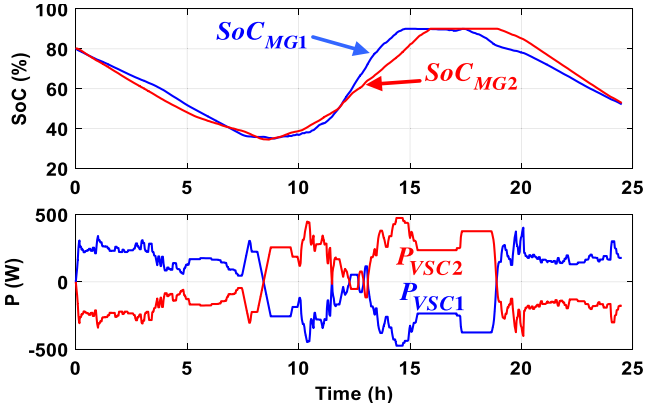

Fig. 13. Comparing the SoC levels in both microgrids and the power exchange through the multiterminal converter.

$Sign(P_{ESS_{MG2}})$). The first one is mapped using 5 MFs with the same labels as in Section 3.1, and the mapping is illustrated in Fig. 14(a). The second and third inputs are directly obtained from the sign function, resulting in two MFs labeled Positive (P) and Negative (N), as shown in Fig. 14(b). Finally, the output of the FIS is the same incremental

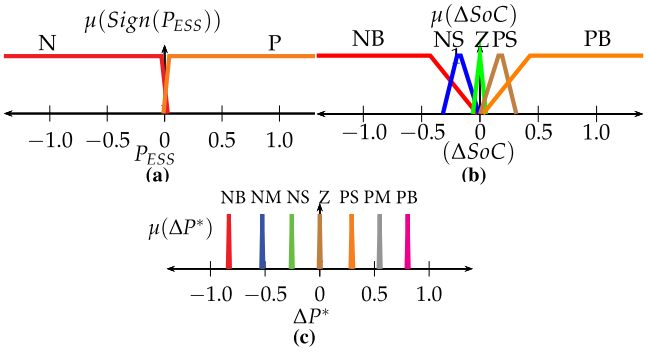

Fig. 14. Fuzzy sets for the simplified FIS.

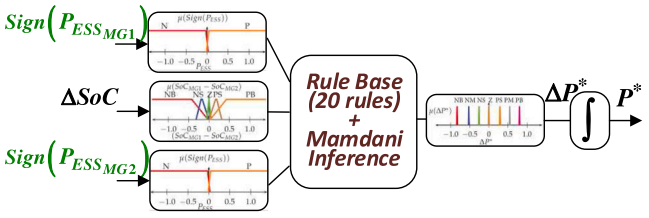

Fig. 15. Scheme of the simplified fuzzy controller.

Table 3
Rule base of the simplified FIS.

		$Sign(P_{ESS_{MG1}})$			
		N		P	
ΔSoC	PB	PB	PB	PS	PM
	PS	PS	PM	Z	PM
	Z	Z	PS	NS	Z
	NS	NM	Z	NB	NM
	NB	NM	NS	NB	NM
		N	P	N	P
		$Sign(P_{ESS_{MG2}})$			

variable (ΔP^*), with the same number and mapping of MFs defined in Section 3.1, as depicted in Fig. 14(c).

As a result, the rule base of the FIS has been reduced to only 20 rules, which is a significant improvement in computational efficiency. These rules consist of 5 for ΔSoC, 2 for $Sign(P_{ESS_{MG1}})$, and 2 for $Sign(P_{ESS_{MG2}})$, resulting in a total of 20 *If-Then* rules. This simplification provides a more objective and general solution with a clear control objective, which is the SoC equalization. Fig. 15 shows the scheme of the simplified FIS that will be implemented in the Energy Exchange Management Unit. Table 3 maps the 20 rule-base combinations derived from the simplified FIS.

Fig. 16 shows the simulation response of MG1 (Fig. 16(a)) and MG2 (Fig. 16(b)) when the VSC is controlled by the simplified FIS in the energy exchange management unit. The following remarks can be extracted from these results:

(a) Similarly to the operation with the former FIS, there is no load disconnection.

(b) A better use of RES is achieved since no power generation curtailment takes place in MG2. In quantitative terms, the energy curtailed is **52% less** compared to the case of microgrids independent operation and **16% less** than with the former FIS.

Additionally, Fig. 17 shows the comparison between the SoC profiles and the power exchanged through the two-terminal conversion stage for each microgrid, confirming the SoC profiles' equalization. Therefore, it can be concluded that the modified cooperative strategy leads to a better overall performance of the integrated microgrids.

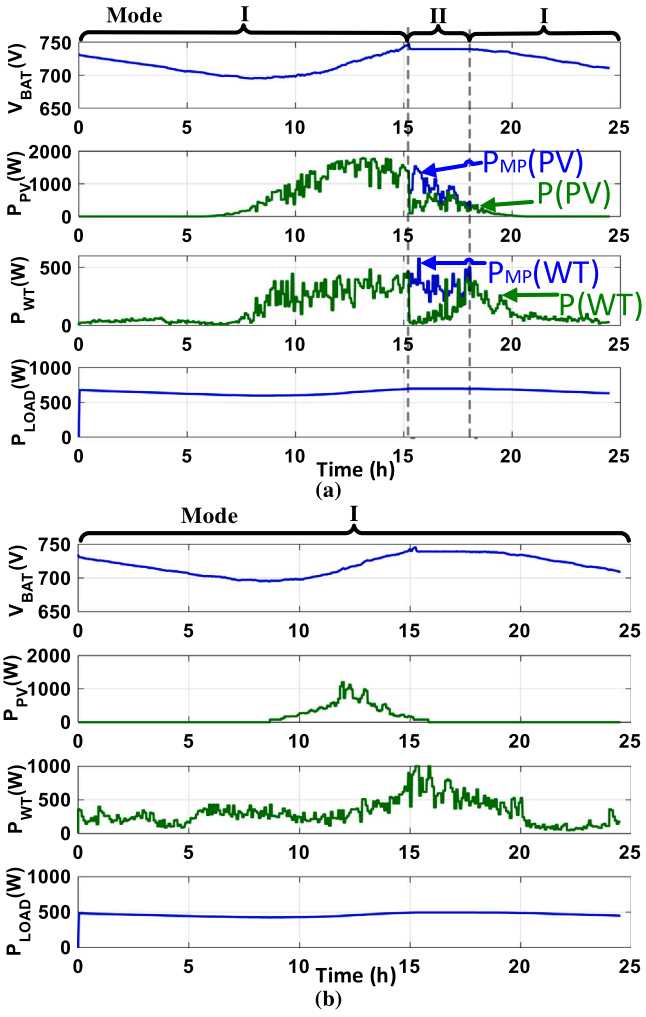

Fig. 16. Operation with the simplified fuzzy energy exchange strategy: (a) MG1, (b) MG2.

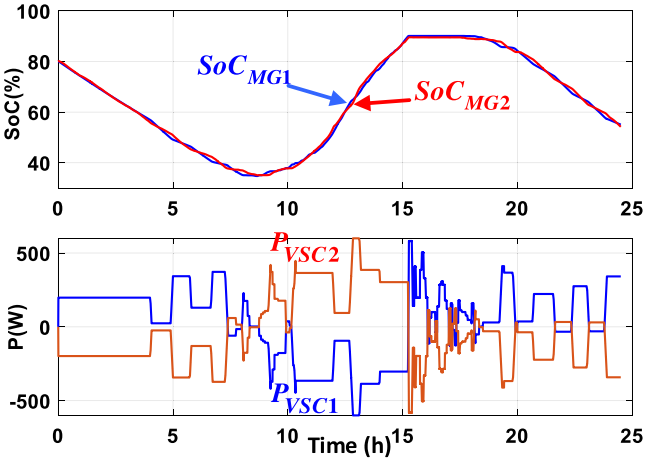

Fig. 17. Comparison between SoC in both microgrids and power exchanged through the multiterminal converter.

3.3. Proof and considerations for expandability to more than two microgrids

In order to test the expandability of the proposed strategy, a third microgrid (MG3) has been connected to the dc-bus of the VSC-based Multiterminal stage. For this third microgrid, the same PV profile as in MG1 is used, and the same WT profile as in MG2 is used. Nevertheless, at the Energy Exchange Management a copy of the FIS, such as the one shown in Fig. 15 is added. This copy of the FIS is added to set the power reference that should be exchanged by MG3. The new FIS takes three inputs: ($\Delta SoC = SoC_{MG1} - SoC_{MG3}$), $Sign(P_{ESS_{MG1}})$, and $Sign(P_{ESS_{MG3}})$. These inputs allow for equalization with the microgrid connected to the VSC responsible for the dc-bus regulation (in this case, MG1).

Here, it is important to consider that the VSC connected to MG1 is responsible for keeping the power balance in the dc-bus, by means of its regulation. Meanwhile, MG2 and MG3 absorb or inject power to the dc-bus in accordance with the power reference defined by their FISs. Therefore, it is possible that the sum of power injected or absorbed by MG2 and MG3 surpasses the maximum power allowed for the VSC of MG1. Moreover, this problem could increase if more microgrids are linked to the Multiterminal converter.

To deal with this problem, a supervisory control is proposed to avoid that the total power flow managed by the VSC of MG1 exceeds its maximum limits. The supervisory stage will curtail the power references (P^*_{VSCn}) defined by their corresponding FIS for each nth VSC integrated to the DC bus, weighting them by curtailment indexes α_n in such a way that,

$$\sum_{i=1}^{n} \alpha_i * \left| P^*_{VSCi} \right| = P_{max} \tag{3}$$

where, n is the number of microgrids connected to the regulated dc-bus, and P_{max} is the maximum power allowed to managed by the VSC responsible for the dc-bus regulation. This curtailment will be applied only when the sum of all the references surpass the power limit (P_{max}). Additionally, in order to ensure that the power curtailment will be inversely proportional to the power references and then, reduce the effect over the SoC equalization, the following relations are considered.

$$\frac{P^*_{VSC2}}{P^*_{VSC3}} = \frac{\alpha_2}{\alpha_2}, \frac{P^*_{VSC3}}{P^*_{VSC4}} = \frac{\alpha_3}{\alpha_4}, \cdots \frac{P^*_{VSC(n-1)}}{P^*_{VSCn}} = \frac{\alpha_{n-1}}{\alpha_n}. \tag{4}$$

The supervisory stage will calculate the curtailment indexes just by solving the linear system defined by Eqs. (3) and (4). Figs. 18(a) and 18(b) show the performance comparison for the SoC profiles when three microgrids are integrated without and with the supervisory stage respectively. In this case, all the microgrids started with different initial SoC (85% for MG1, 75% for MG2, and 65% for MG3), and despite this, the SoCs of MG2 and MG3 tend to equalize the SoC of MG1. Additionally, all the microgrids operate under a partial SoC which means that all of them operate in Mode I without load disconnection or power curtailment.

On the other hand, Figs. 18(c) and 18(d) show the power profiles for P_{VSC1} and $(P_{VSC2} + P_{VSC3})$ without and with the supervisory stage respectively. As can be seen, the VSC1 balances the power demanded by VS2 and VSC3. Also, it is possible to see that more power is required at the beginning of the simulation in order to perform the SoC equalization. At this point, the system with the supervisory stage (Fig. 18(d)) limits the maximum power to ±2200 W, which is the maximum power allowed for the VSCs, while the system without the supervisory stage excess the maximum power for the VSC1. Finally, from the results in can be said that the supervisory stage does not affect the equalization of the SoCs.

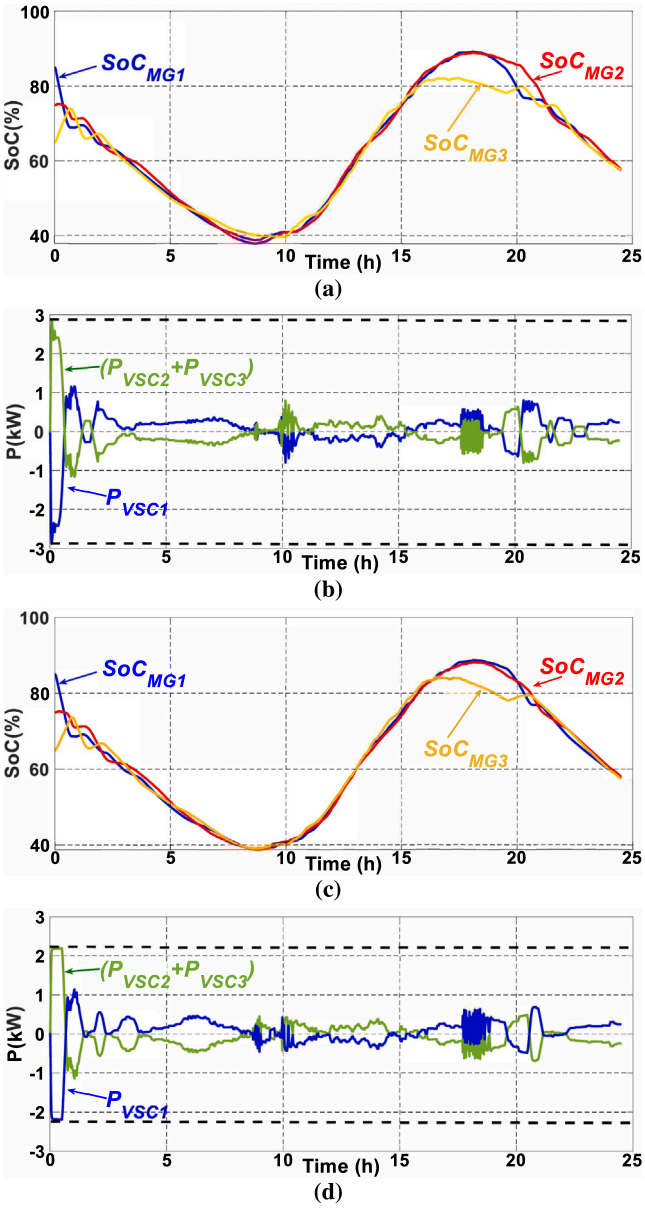

Fig. 18. The SoC and power exchanged profiles for 3 microgrids (a) and (b) without the supervisory stage, (c) and (d) with the supervisory stage.

4. Experimental validation

The experimental validation has been performed in the Microgrid Research Laboratory (MGLab) at Aalborg University by using two experimental microgrids. The laboratory is equipped with multiple setups that include four 2.2 kW Danfoss inverters, LCL filters, measurement LEM sensors, and resistive loads. The inverters in each setup are controlled by a real-time simulation platform (dSPACE1006 control board), which is able to embed the controllers, battery models, and renewable generation profiles.

In this experiment, two setups were used, as shown in Figs. 19 and 20. The parameters of the experimental microgrids and their components are listed in Table 1. The renewable energy source (RES) generation units (PV and WT), the energy storage system (ESS) unit, and the corresponding VSC of the Multiterminal stage were configured for each setup, as shown in Fig. 19. The link between the two AC microgrids was established by connecting two inverters via the DC side. Finally, the control of the VSC, including regulation of the intermediate

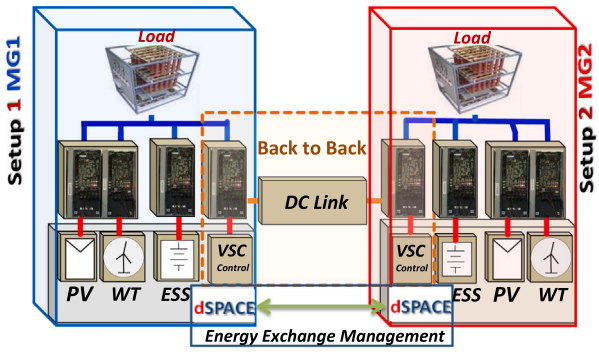

Fig. 19. Configuration of the experimental setup.

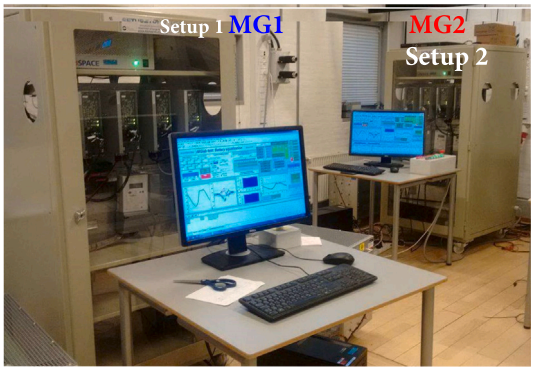

Fig. 20. Image of the experimental laboratory MGLab.

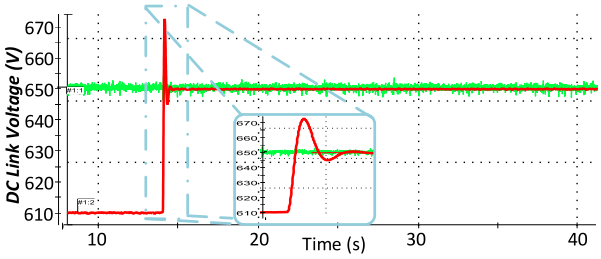

Fig. 21. Response of the intermediate dc-bus control.

DC-bus and energy exchange management, was centralized on one of the dSPACE real-time simulation platforms.

Fig. 21 shows the response of the control of the intermediate DC Bus. The control was activated at 14 s and regulated the DC Bus voltage at 650 V throughout the operation of the integrated systems, enabling power exchange between microgrids.

The main difference between the simulation and the experiment is that load consumption and WT generation profiles have been increased by 500 W (due to the available experimental load). Additionally, Figs. 22(a) and 22(b) show the experimental response of MG1 and MG2, respectively, with the cooperative fuzzy energy exchange strategy. The results confirm that neither load disconnection nor power curtailment occurs in MG2, which is consistent with the simulation results shown in Fig. 16.

Furthermore, Fig. 23 compares the SoC profiles and the power exchanged through the conversion stage, demonstrating how the SoC profiles in both microgrids tend to be equalized, as established by the strategy. Moreover, the figure indicates that the power delivered by one microgrid is approximately the same as that absorbed by the other one.

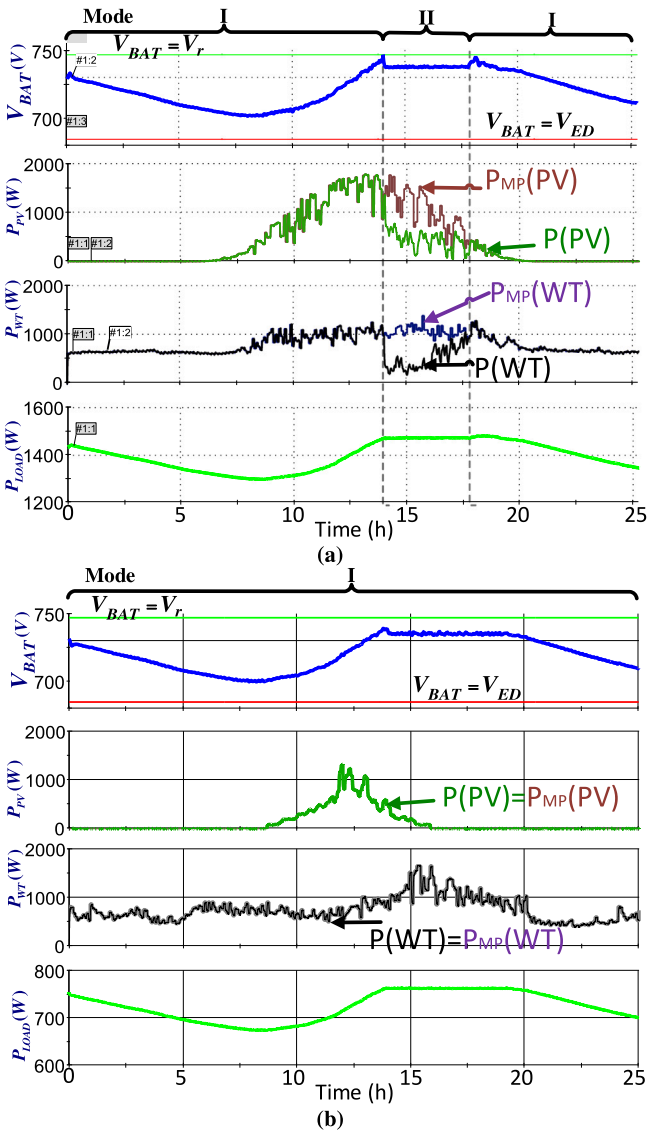

Fig. 22. Experimental results for the integrated system: (a) (MG1), (b) (MG2).

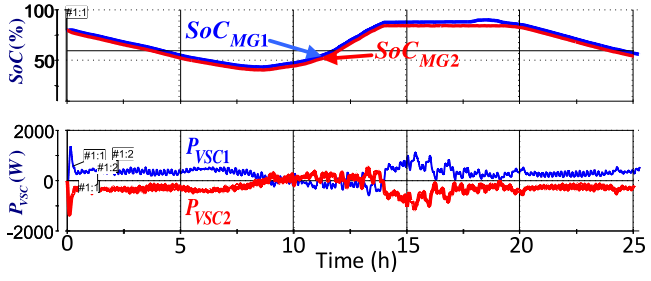

Fig. 23. Experimental comparison between SoCs and power exchanged through the multiterminal converter.

Fig. 24 shows the response of the voltage in the dc-bus where it can be seen how the dc-bus is regulated around 650 V despite the power exchanged through the dc-bus.

5. Conclusion

This paper proposes a comprehensive cooperative power exchange strategy between stand-alone microgrids through a multiterminal power

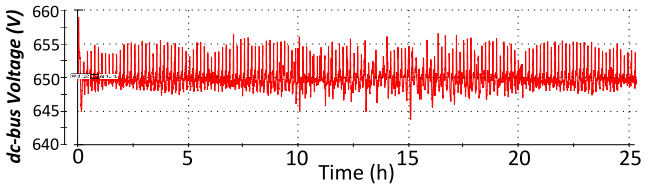

Fig. 24. Interlink dc-bus voltage during the experiment.

stage based on VSCs. The proposed strategies are based on fuzzy inference systems to take advantage of the ease of defining a strategy through linguistic sentences and the robustness in the face of parameter uncertainties and stochastic behavior of RES. Initially, a FIS was developed based purely on qualitative knowledge, resulting in an extensive rule-base that achieves the primary goal of improving the global reliability of the integrated stand-alone microgrids in terms of load supply and greater utilization of available renewable energy power. From this first strategy, specific control objectives were clarified, and a simplified FIS with better performance and less computational complexity was defined.

The proposed strategy has been shown to be completely expandable, allowing for the integration of more microgrids through VSC units connected to a common DC-bus. In this sense, the use of more than one unit sharing the responsibility of DC voltage regulation can be considered as an alternative for increasing the rate of exchanged power between VSCs and enabling the integration of more microgrids. Additionally, changes in the control modes of the VSCs should be considered to provide more flexibility and reconfigurability to the operation of the multiterminal converter.

On the other hand, the simplicity of defining the linguistic fuzzy model is counteracted by the tuning of the fuzzy sets. The current work follows several research axes. The first of which treats the tuning of the fuzzy sets as a pure optimization problem, as seen in [46,47]. The second axis involves studying how including forecast information in the FIS can improve the overall system response, using approaches such as the one suggested in [48]. Finally, the extension of this approach to strategies that consider other trade rules instead of cooperative operation is also envisioned.

CRediT authorship contribution statement

Nelson L. Díaz: Conception and design of study, Acquisition of data, Analysis and/or interpretation of data, Writing – original draft, Writing – review & editing. **Francesc Guinjoan:** Conception and design of study, Analysis and/or interpretation of data, Writing – original draft, Writing – review & editing. **Guillermo Velasco-Quesada:** Conception and design of study, Analysis and/or interpretation of data. **Adriana C. Luna:** Acquisition of data, Analysis and/or interpretation of data, Writing – original draft, Writing – review & editing. **Josep M. Guerrero:** Acquisition of data, Writing – review & editing.

Declaration of competing interest

The authors declare that they have no known competing financial interests or personal relationships that could have appeared to influence the work reported in this paper.

Data availability

Data will be made available on request.

References

[1] Xie R, Wei W, Shahidehpour M, Wu Q, Mei S. Sizing renewable generation and energy storage in stand-alone microgrids considering distributionally robust shortfall risk. IEEE Trans Power Syst 2022;37(5):4054–66.
[2] Zahira R, Lakshmi D, Ezhilarasi G, Sivaraman P, Ravi C, Sharmeela C. 6 - stand-alone microgrid concept for rural electrification: a review. In: Padmanaban S, Sharmeela C, Sivaraman P, Holm-Nielsen JB, editors. Residential microgrids and rural electrifications. Academic Press; 2022, p. 109–30.
[3] Schnitzer D, Lounsbury DS, Carvallo JP, Deshmukh R, Apt J, Kammen DM. Microgrids for rural electrification: A critical review of best practices based on seven case studies. United Nations Found. 2014.
[4] Kumar NP, Makai L, Singh M, Cho H, Dauenhauer P, Mutale J. Analyzing sub-optimal rural microgrids and methods for improving the system capacity and demand factors: Filibaba microgrid case study examined. In: 2017 IEEE global humanitarian technology conference. 2017, p. 1–8.
[5] Guan Y, Wei B, Guerrero JM, Vasquez JC, Gui Y. An overview of the operation architectures and energy management system for multiple microgrid clusters. iEnergy 2022;1(3):306–14.
[6] Susanto J, Shahnia F, Ghosh A, Rajakaruna S. Interconnected microgrids via back-to-back converters for dynamic frequency support. In: 2014 Australasian universities power engineering conference. 2014, p. 1–6.
[7] Liu W, Gu W, Xu Y, Wang Y, Zhang K. General distributed secondary control for multi-microgrids with both PQ-controlled and droop-controlled distributed generators. IET Gener Transm Distrib 2017;11(3):707–18.
[8] Pashajavid E, Ghosh A, Zare F. A multimode supervisory control scheme for coupling remote droop-regulated microgrids. IEEE Trans Smart Grid 2018;9(5):5381–92.
[9] Nutkani IU, Loh PC, Wang P, Jet TK, Blaabjerg F. Intertied ac–ac microgrids with autonomous power import and export. Int J Electr Power Energy Syst 2015;65:385–93.
[10] Bala S, Venkataramanan G. Autonomous power electronic interfaces between microgrids. In: 2009 IEEE energy conversion congress and exposition. 2009, p. 3006–13.
[11] Nutkani IU, Loh PC, Blaabjerg F. Distributed operation of interlinked AC microgrids with dynamic active and reactive power tuning. IEEE Trans Ind Appl 2013;49(5):2188–96.
[12] Kumar M, Srivastava SC, Singh SN, Ramamoorty M. Development of a control strategy for interconnection of islanded direct current microgrids. IET Renew Power Gener 2015;9(3):284–96.
[13] Bullich-Massagué E, Díaz-González F, Aragűés-Peñalba M, Girbau-Llistuella F, Olivella-Rosell P, Sumper A. Microgrid clustering architectures. Appl Energy 2018;212:340–61.
[14] Che L, Shahidehpour M, Alabdulwahab A, Al-Turki Y. Hierarchical coordination of a community microgrid with AC and DC microgrids. IEEE Trans Smart Grid 2015;6(6):3042–51.
[15] Majumder R, Ghosh A, Ledwich G, Zare F. Power management and power flow control with back-to-back converters in a utility connected microgrid. IEEE Trans Power Syst 2010;25(2):821–34.
[16] Zhang X, Cheng S, Zhang P, Zeng G. Frequency and amplitude modulation with back to back converters in a utility connected microgrid. In: 2015 Chinese automation congress. 2015, p. 1389–93.
[17] McCann NSR. Energy shaping control of a back-to-back converter for microgrid applications. In: 2017 IEEE power energy society general meeting. 2017, p. 1–5.
[18] Martins MAI, Pica CQ, Maryama V, Pacheco B, Heldwein ML, da Silva Jr JNR. Design and implementation of a microgrid power management unit using a back-to-back converter in a residential condominium connected at medium voltage. In: 2015 IEEE 13th Brazilian power electronics conference and 1st southern power electronics conference. 2015, p. 1–5.
[19] Wang H, Redfern MA. The advantages and disadvantages of using HVDC to interconnect ac networks. In: 45th international universities power engineering conference. 2010, p. 1–5.
[20] Ye Y, Qiao Y, Xie L, Lu Z. A comprehensive power flow approach for multi-terminal VSC-HVDC system considering cross-regional primary frequency responses. J Mod Power Syst Clean Energy 2020;8(2):238–48.
[21] Nutkani IU, Loh PC, Blaabjerg F. Power flow control of intertied ac microgrids. IET Power Electron. 2013;6(7):1329–38.
[22] Yoo H-J, Nguyen T-T, Kim H-M. Multi-frequency control in a stand-alone multi-microgrid system using a back-to-back converter. Energies 2017;10(6).
[23] Naderi M, Khayat Y, Shafiee Q, Dragicevic T, Bevrani H, Blaabjerg F. Interconnected autonomous AC microgrids via back-to-back converters part I small-signal modeling. IEEE Trans Power Electron 2020;35(5):4728–40.
[24] Mohammed SR, Teh J, Kamarol M. Upgrading of the existing bi-pole to the new four-pole back-to-back HVDC converter for greater reliability and power quality. IEEE Access 2019;7:145532–45.
[25] Dong W, Yang Q, Fang X, Ruan W. Adaptive optimal fuzzy logic based energy management in multi-energy microgrid considering operational uncertainties. Appl Soft Comput 2021;98:106882.

[26] Sinha S, Tekumalla DV, Bajpai P. Fuzzy logic controlled power sharing among energy storage devices in multiple standalone DC microgrids. In: 2019 IEEE PES innovative smart grid technologies Europe. 2019, p. 1–5.
[27] Du Y, Wang Z, Liu G, Chen X, Yuan H, Wei Y, et al. A cooperative game approach for coordinating multi-microgrid operation within distribution systems. Appl Energy 2018;222:383–95.
[28] Mo S, Chen W-H, Lu X. Distributed hybrid secondary control strategy for DC microgrid group based on multi-agent system. In: 2021 33rd Chinese control and decision conference. 2021, p. 109–14.
[29] Al Sumarmad KA, Sulaiman N, Wahab NIA, Hizam H. Energy management and voltage control in microgrids using artificial neural networks, PID, and fuzzy logic controllers. Energies 2022;15(1).
[30] Elmouatamid A, Ouladsine R, Bakhouya M, El Kamoun N, Khaidar M, Zine-Dine K. Review of control and energy management approaches in micro-grid systems. Energies 2021;14(1).
[31] Mlakić D, Baghaee HR, Nikolovski S. A novel ANFIS-based islanding detection for inverter-interfaced microgrids. IEEE Trans Smart Grid 2019;10(4):4411–24.
[32] Wu D, Tang F, Dragicevic T, Vasquez JC, Guerrero JM. Autonomous active power control for islanded AC microgrids with photovoltaic generation and energy storage system. IEEE Trans Energy Convers 2014;29(4):882–92.
[33] Rocabert J, Luna A, Blaabjerg F, Rodríguez P. Control of power converters in AC microgrids. IEEE Trans Power Electron 2012;27(11):4734–49.
[34] Katiraei F, Iravani R, Hatziargyriou N, Dimeas A. Microgrids management. IEEE Power Energy Mag 2008;6(3):54–65.
[35] Diaz NL, Dragičević T, Vasquez JC, Guerrero JM. Intelligent distributed generation and storage units for DC microgrids—A new concept on cooperative control without communications beyond droop control. IEEE Trans Smart Grid 2014;5(5):2476–85.
[36] Díaz NL, Luna AC, Vasquez JC, Guerrero JM. Centralized control architecture for coordination of distributed renewable generation and energy storage in islanded AC microgrids. IEEE Trans Power Electron 2017;32(7):5202–13.
[37] Granados Hernández ED, Díaz Aldana NL, Luna Hernández AC. Energy management electronic device for islanded microgrids based on renewable energy sources and battery-based energy storage. Ingeniería e Investigación 2021;41(1):e83905.
[38] IEEE Power and Energy Society. IEEE standard for the specification of microgrid controllers. 2017, p. 1–42, IEEE Std 2030.7-2017.
[39] Marra F, Yang G. Chapter 10 - decentralized energy storage in residential feeders with photovoltaics. In: Lu PD, editor. Energy storage for smart grids. Boston: Academic Press; 2015, p. 277–94.
[40] Buchmann I, Inc CE. Batteries in a portable world: A handbook on rechargeable batteries for non-engineers. 4th ed. Cadex Electronics; 2016.
[41] Lopes JAP, Moreira CL, Madureira AG. Defining control strategies for MicroGrids islanded operation. IEEE Trans Power Syst 2006;21(2):916–24.
[42] IEEE guide for optimizing the performance and life of lead-acid batteries in remote hybrid power systems. 2008, p. C1–25, IEEE Std 1561-2007.
[43] Lee W-G, Nguyen T-T, Yoo H-J, Kim H-M. Consensus-based hybrid multiagent cooperative control strategy of microgrids considering load uncertainty. IEEE Access 2022;10:88798–811.
[44] Babuka R. Fuzzy systems, modeling and identification. 1998.
[45] Passino KM, Yurkovich S. Fuzzy control. Addison Wesley Longman; 1998,
[46] García-Gutiérrez G, Arcos-Aviles D, Carrera EV, Guinjoan F, Motoasca E, Ayala P, et al. Fuzzy logic controller parameter optimization using metaheuristic cuckoo search algorithm for a magnetic levitation system. Appl Sci 2019;9(12):2458.
[47] Faisal M, Hannan MA, Ker PJ, Uddin MN. Backtracking search algorithm based fuzzy charging-discharging controller for battery storage system in microgrid applications. IEEE Access 2019;7:159357–68.
[48] Arcos-Aviles D, Pascual J, Guinjoan F, Marroyo L, Sanchis P, Marietta MP. Low complexity energy management strategy for grid profile smoothing of a residential grid-connected microgrid using generation and demand forecasting. Appl Energy 2017;205:69–84.